

Analysis of Stainless Steel Bipolar Plates Micro-Stamping Processes

Abstract. Bipolar plate is one of the key components of proton exchange membrane fuel cells (PEMFC). Since the production costs of traditional graphite bipolar plates are very expensive and need a few millimeters thickness over the space, the resulting metal bipolar plate not only reduces the cost of such a bipolar plate, the thickness can also be reduced to micron range. This study aims to explore the application of micro-stamping technology to produce thin metal bipolar plates with the relevant process parameters. Regarding the use of rigid punch on 50 μ m-thick stainless steel sheet (SUS 304) for micro-channel stamping process in this study, the channel design is 0.8*0.75mm. Besides, the finite element method and the experimental results are used to analyze the micro-stamping process key parameters. In this study, traditional material model and the scale-factor modified material model are used for simulation. The experimental results verified by the modified material model are more realistic to products and have better similarity, as the punch load is relatively small. The results demonstrate that the use of micro-stamping production of thin metal bipolar plates could not only reduce the production cost, but could also speed up the process. In this paper, using ULF (updated Lagrangian formulation) concept to establish an elastic-plastic deformation finite element analysis model and using scale-factor to modify the calculation could effectively simulate the micro-stamping process for metal bipolar plates.

Streszczenie. Dwubiegunowa płyta jest zasadniczym składnikiem baterii PEMFC z membranową wymianą protonową. W artykule zaproponowano zastąpienie tradycyjnej płyty grafitowej przez płytę oraz opisano technologię mikro-tłoczenia w celu uzyskania grubości rzędu mikronów. (Analiza procesu mikro-tłoczenia stosowane go do otrzymywania stalowych bipolarnych membran o ekstremalnie małych grubościach)

Keywords: Micro-stamping, Bipolar plate, Stainless steel, PEMFC.

Słowa kluczowe: mikro-tłoczenie, baterie z wymianą protonową

1. Introduction

Proton exchange membrane fuel cell, as a potential emerging alternative energy, has been widely used in transportation system, cogeneration system, and set-based power generation system, because of its high efficiency, high power density, and system stability, etc. [1]-[3]. However, with various components of fuel cells, the bipolar plate is the most important, about 60-80% of the stack weight, about 50% of the stack volume, and approximately 35-45% of stack costs [4]-[6]. For this reason, when the cost of bipolar plates is reduced, fuel cells will be widely used. In recent years, many scholars turned to the study on having corrosion-resistant metal bipolar plates replaced the graphite bipolar plates, mainly because the cost for metal bipolar plate manufacturing was lower than it for the traditional graphite plates, as well as on the development of small forms [7]. Two problems have shown on current production of metal bipolar plates. (1) Poor corrosion resistance of metal plates can cause oxidation and decline the performance of MEA. (2) The breakthrough manufacturing technology is lack for the high efficiency, low cost, and high-precision thin metal bipolar plate process [8].

The sheet metal forming process has gradually replaced the past processing methods. Regarding sheet metal, stamping and hydraulic processes are considered the most efficient way to meet the future demand of mass production. In previous academic results, the full proof of stamping process could be effective in thin metal plate making a micro-channel, and could serve as an alternative to the production of metal bipolar plates [9]. Linfa Peng and Peng Hu proposed that micro-stamping process for bipolar plates could improve production efficiency [10].

However, in previous studies, there was no clear indication of the finite element method analysis for micro-sheet metal stamping process. Therefore, this paper presented the traditionally macro material stress-strain model and micro scale-factor modified stress-strain model, a different finite element analysis model, to explore the micro-stamping stainless steel sheet process. The results showed that the proportion of the thickness scale-factor could effectively simulate the micro sheet metal forming process.

2. Basic Theory

2.1. Stiffness Equation

The equation for virtual work can be made discrete. The updated Lagrangian formulation (ULF) in the application of an incremental deformation for metal forming process (bulk forming and sheet forming) can be practically applied to describe the incremental properties of plastic flow. The current configuration, according to the deformation of ULF at each stage, is used as a reference state to evaluate the deformation during a small time interval Δt , such that first-order theory is consistent with the required accuracy.

The rate equation for virtual work, written as an updated Lagrangian equation [11], is

$$(1) \int_{V^E} (\dot{\sigma}_{ij} - 2\sigma_{ik} \dot{\epsilon}_{kj}) \delta \epsilon_{ij} dV + \int_{V^E} \sigma_{jk} L_{ik} \delta L_{ij} dV = \int_{S_f} \dot{f} \delta v_i dS$$

in which v_i is the velocity, \dot{t}_i is the rate of the nominal traction, and V and S_f represent the material volume and the surface on which the traction is prescribed.

Since the rate equation for the virtual work and the constitutive relation are linear equations of rates, they can be replaced with increments defined with respect to any monotonously increasing measure, such as the increase in the displacement of the tool.

Applying the standard procedure of finite elements to form the complete global stiffness matrix, it yields

$$(2) [K] \{\Delta u\} = \{\Delta F\}$$

in which,

$$(3) [K] = \sum_{\langle E \rangle} \int_{V^E} [B]^T ([C^{ep}] - [Q])[B] dV + \sum_{\langle E \rangle} \int_{V^E} [E]^T [Z][E] dV$$

In these equations, the term $\{\Delta u\}$ represents the increment in nodal displacement and $\{\Delta F\}$ is the prescribed increase in nodal force. $[K]$ represents the global tangent stiffness matrix; $[C^{ep}]$ is the elemental elastic-plastic constitutive matrix; $[B]$ is the strain rate velocity matrix; and $[E]$ is the velocity gradient-velocity matrix. Matrices $[Q]$ and $[Z]$ are defined as stress correction matrices associated with the stress states during each deformation stage.

2.2. Selective Reduced Integration Formulation

The volume of a plastic medium is incompressible. Therefore, implementing the full integration technique for finite elements leads to over-strong constraint on thin plates. This phenomenon is caused by setting the shear strains γ_{xz} and γ_{yz} to zero during deformation [12]. The selective reduced integration (SRI) procedure has been proven to effectively treat such problems as those involving volumetrically stiff contribution [13]. The generalized formulation of SRI, due to Hughes [14], was used to develop the finite element program in this study, which used a four-node shell element.

2.3. Scale-Factor for Sheet Metal Micro-Forming Process

When the thickness of the sheet metal is larger than 1.0mm, the size effect can be neglected; while the thickness is less than 1.0mm, the size effect then becomes crucial. For micro-forming process the thickness of sheet metals is in micron range that the existed size effect makes traditional material model not suitable for micro-forming process. As a result, a new material model needs to be established for micro-stamping process. Traditional Swift material model (without considering size effect) was first applied in this study.

$$(4) \quad \bar{\sigma} = K(\bar{\epsilon}_0 + \bar{\epsilon}_p)^n$$

The applied sheet metal thickness was $50\mu\text{m}$, which was regarded as micro-forming process so that size effect should be taken into account. The thickness of sheet metal is taken into traditional material model for stress-strain relations amendment. Consequently, (4) was amended as follows.

$$(5) \quad \bar{\sigma}(t, \bar{\epsilon}) = aK e^{bt} (\bar{\epsilon}_0 + \bar{\epsilon}_p)^{n(c e^{dt} - 1)}$$

where a, b, c, d are the correction values and t is sheet thickness.

The values for a, b, c, d , obtained from the research results of Fang Liu [15], were substituted in (5). Then,

$$(6) \quad \bar{\sigma}(t, \bar{\epsilon}) = 0.73667Ke^{0.3152t} (\bar{\epsilon}_0 + \bar{\epsilon}_p)^{n(1.0106e^{-0.01029t} - 1)}$$

Traditional material model (4) and the modified material model (6) were proceeded finite element analyses in this study. Experiments were further implemented to verify the differences between the two models.

3. Numerical Analysis

This study used quadrilateral four-node shell element to derive the stiffness matrix and CAD software package for processing model. Due to model symmetry, 1/4 analysis simulation model was adopted to save the computation time. Sheet metal mesh processing was done in the CAD software, converted into data files, and inputted to the 3D elastic-plastic finite element numerical analysis program. The analysis of the simulated output to the CAD software, with further interpretation of the software, could show the deformation figures and the distribution of stress and strain. In this study, material properties, as shown in Table 1, contained the relationship between equivalent stress and equivalent strain. In the material table, there are two material parameters in macro material model for traditional and modified micro scale-factor model.

This study mainly discussed the differences between two material models and the experimental results as well as observed the deformation of sheet metal bipolar plates in micro-stamping process. The geometric configuration of the tools and the distribution of simulating configuration are shown in Fig. 1, where $R_d=0.2\text{mm}$, $R_p=0.15\text{mm}$, $W=0.80\text{mm}$, $h=0.75\text{mm}$, and tools gap $60\mu\text{m}$.

Table 1. Mechanical properties of the SUS304 sheet employed in the forming process

Material (SUS304)	$E(\text{GPa})$	ν	$\sigma_y(\text{MPa})$	$K(\text{MPa})$	n	$\bar{\epsilon}_0$
Tradition	207	0.3	415	1819	0.576	0.077
Scale-factor	207	0.3	306	1361	0.582	0.077

The true stress-strain curve is approximated by $\bar{\sigma} = K(\bar{\epsilon}_0 + \bar{\epsilon}_p)^n$; E : Young's modulus; ν : Poisson's ratio and σ_y : yield stress.

In this study, L1 section and L2 section were used to measure the thickness and the shape, as shown in Fig. 2. Comparisons of different material models in the micro-stamping sheet metal process were demonstrated. In the simulation, the blank must be added to the appropriate boundary conditions, which must be set in the node. This simulated set of boundary conditions in blank X-axis's nodes had to limit the displacement in Y-direction and the rotation in Z-direction. In addition, Y-axis's nodes were required to limit the displacement in X-direction and the rotation in Z-direction.

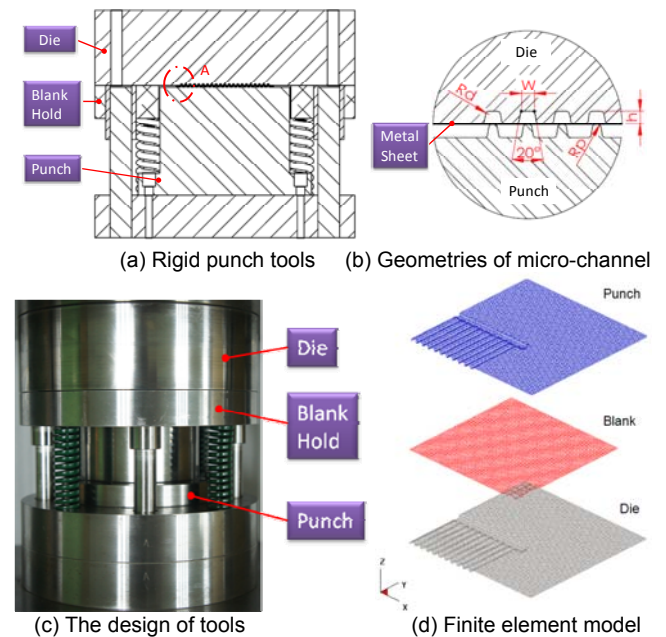


Fig. 1. Micro-stamping process to manufacture micro-channel on the stainless steel bipolar plates and finite element model.

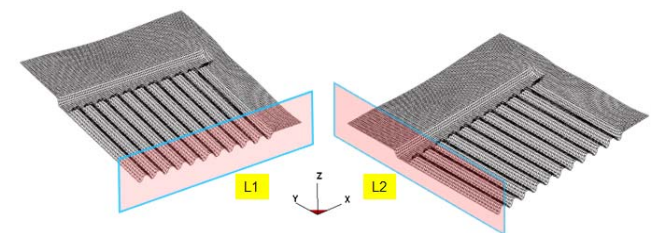


Fig. 2. Measurement diagram.

3.1. Boundary Conditions

The contact, or otherwise made by each node, varied with the deformation of the blank. Therefore, during the calculation of the increase in displacement, the normal component of the contacting node force must be checked to determine whether it was less than or equal to zero. The next step in the calculation of the increase in the displacement must be changed; that is, the boundary condition of this node became a free node. The free node must also be checked to determine whether it contacted the tool. If so, in the subsequent step in the calculation of the increase in displacement, the boundary conditions were changed to those of a contacting node. The above calculation was performed with an extended r-minimum.

At the contact interface, the discontinuous alternation between the sliding and sticking states of friction occasionally caused computational difficulty that the treatment of friction conditions required special attention. A modified Coulomb friction law, proposed by Oden and Pries [16] and Saran and Wagoner [17], was assumed involving two contact friction states, sticking and sliding. This friction law effectively specified the discontinuous variation in the direction of sliding. The simulation of micro-stamping process conditioned on the assumption of friction coefficient $\mu=0.05$ to describe the friction condition.

3.2. Elastic-Plastic Problems

The former boundary condition showed that the contact condition remained unaltered within one increment of deformation. Accordingly, the r-minimum method of Yamada et al. [18] was applied and extended to treat elastic-plastic and contact problems.

3.3. Unloading Problems

Spring-back or spring-forward is significant in sheet metal forming. Therefore, the unloading behavior following sheet metal forming was considered. The unloading procedure was executed, and all elements were reset to be elastic. The force with which the nodes contacted the tools was reversed to become the prescribed force boundary condition on the sheet.

$$(7) \quad \Delta f = -f$$

4. Results and Discussions

Fig. 3 shows the different material models in stainless steel sheet as well as the relationship between the punch load and the punch stroke. In the calculation process, when contacting between sheet and tools, the punch load increased rapidly. From the loading simulation, several features were found. In the beginning of formation, the punch load was rapidly increased, and the load curve did not present obvious difference on either traditional or modified material models. Once the punch stroke was increased, the load curve would rapidly rise. In the process of formation, the curve changes of both models were similar. However, the scale-factor modified material model appeared smaller load curve than the traditional material model did.

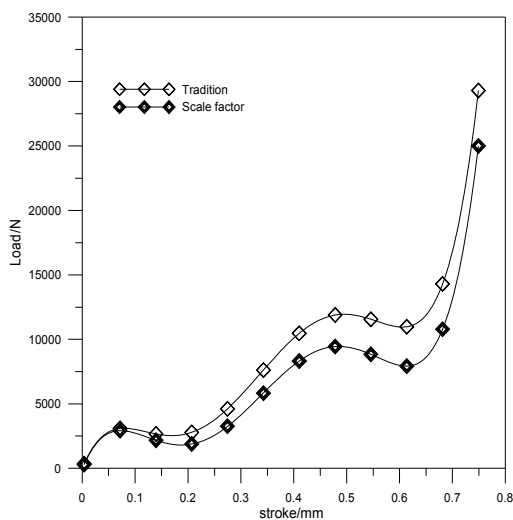


Fig. 3. The punch load and relative punch stroke for different material model.

Fig. 4 shows the geometric deformation of the five stages in the micro-stamping process for sheet metal bipolar plates. Apparently, the sheet metal gradually deformed while stamping. Not until the unloading state,

were the contact, the separation, and the friction calculated with r-minimum rule in the stamping process.

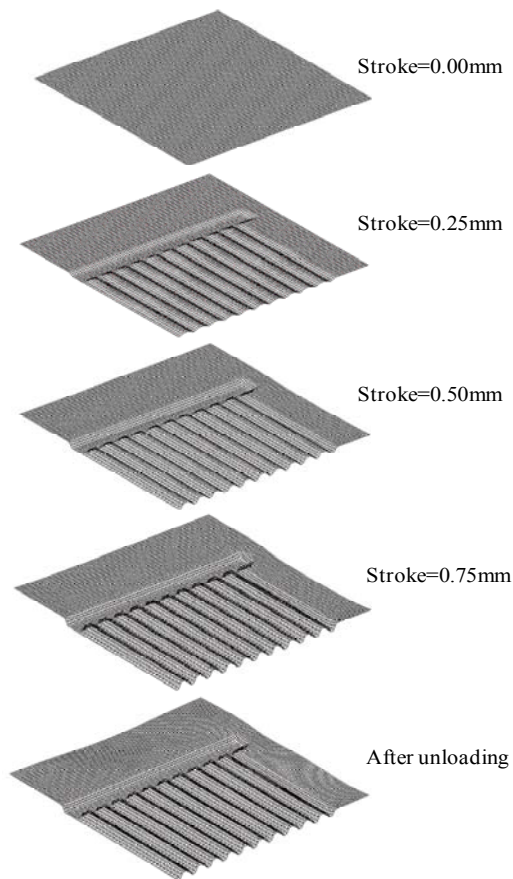


Fig. 4. Micro-stamping process of the geometric deformation.

4.1. Effect of Material Model

In this paper, different material models were used for the analysis of micro-stamping process, and the differences between the two were explored. L1 section and L2 section in the simulated and the experimented sheet metal bipolar plates were utilized to measure the thickness and the shape. With comparisons, the feasibility of the modified material model was further verified.

Based on the analysis, Fig. 5, the thinnest area appeared on the round corners at both ends of the channel. After comparison, the thinnest area of both models appeared on the modified material model, 0.0265mm, which merely presented 0.0005mm difference with the traditional material model. The distribution of the traditional material model was larger than it of the modified material model. With stress distribution, there was stress concentration in the first channel. The reason might be the material flow in the area being more violent. Nonetheless, larger stress appeared on the traditional macro model, 985MPa, which showed 100MPa difference with the modified micro model.

4.2. Experiments of Micro-Stamping

To prove the proposed phenomenon being in accordance with the experimental product, the 50 μ m-thick stainless steel sheet was preceded stamping in the trapezoid channel. The equipment and the tools for the experiment are shown in Fig. 6. The experimental product (Fig. 7) was measured the shape with laser displacement meter. The experimental results were compared with the simulated results; and, the traditional material model and the scale-factor modified material model were further discussed the differences.

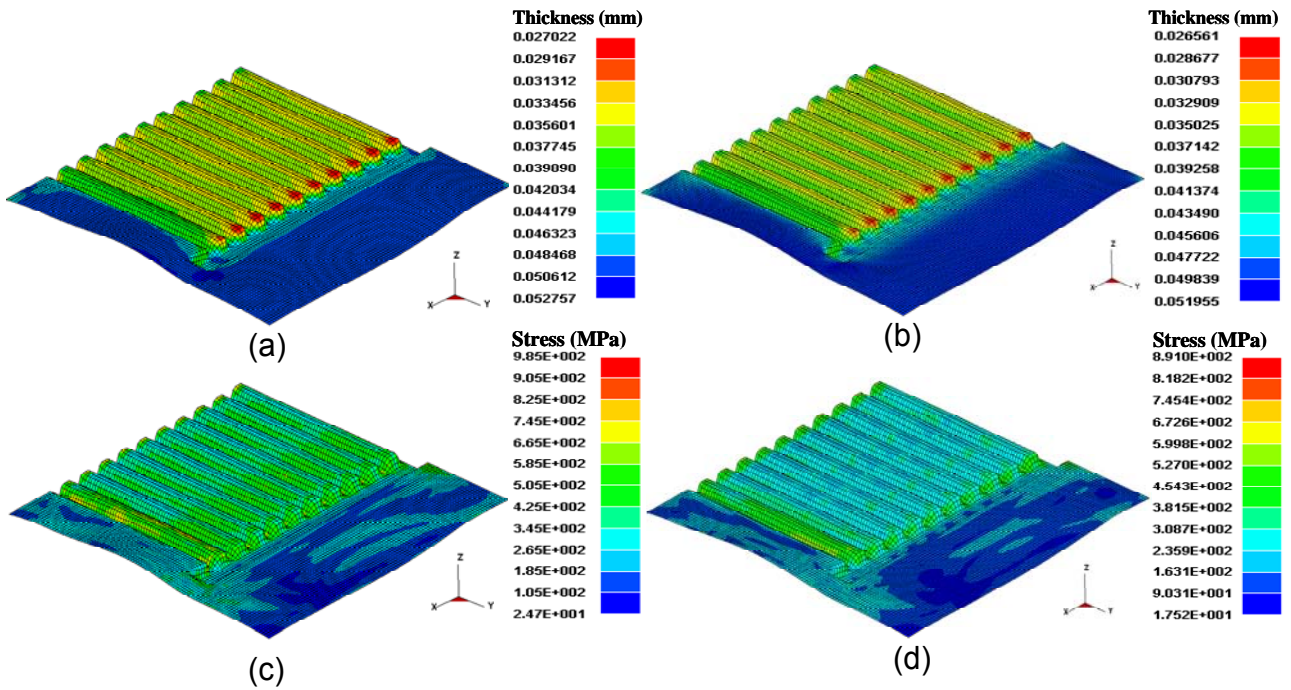
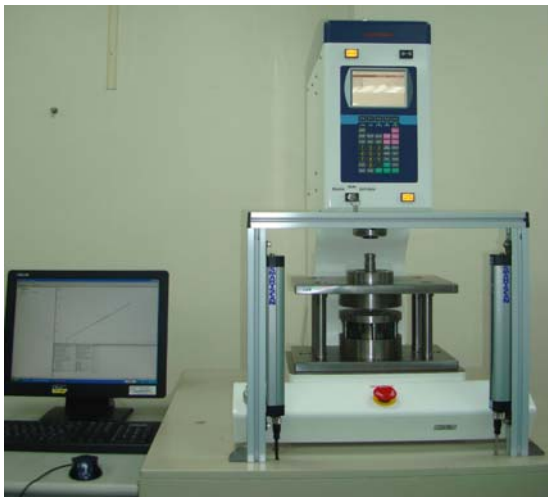


Fig. 5. The results of different material models compare with thickness distribution and stress distribution. (a) Traditional. (b) Modified. (c) Traditional. (d) Modified.



(a)



(b)

Fig. 6. (a) Electronic press (b) Laser displacement meter.

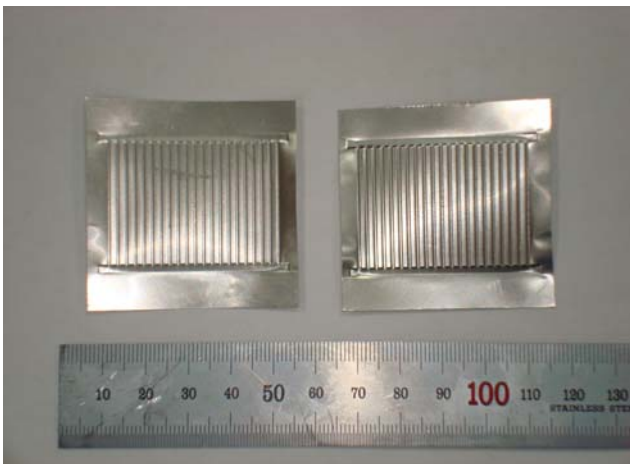


Fig. 7. The photo of formed parts of trapezoid channel.

Fig. 8 displays the thickness distribution of L1 section (X-axis), where the thickness in the channel was between 0.043~0.033mm. The thinnest area appeared on the top of the channel because of the pull on both sides of the channel. Moreover, the thickest area appeared on the bottom of the transverse channel. The thickness distribution in L1 section did not show large differences between the two material models. However, the least thickness of the product and it of the simulation presented obvious differences, after comparison. The error of the thickness distribution on L1 section among the three (traditional material model, modified material model, and experimental result) was small, within reasonable limits. Furthermore, the thickness distribution on L2 section (Y-axis) was also compared, Fig. 9. The largest thickness error of the three (traditional material model, modified material model, and experimental result) appeared on the bottom of the middle of channel, with the thickness close to 0.037mm. The thickness distribution outside the channel was about identical. According to the comparison of the

thickness distribution on the two sections among the two material models and the experimental result, the simulated result of the scale-factor modified material model was close to the experimental result. However, the errors among the three were within the reasonable 5% (from the aspect of engineering).

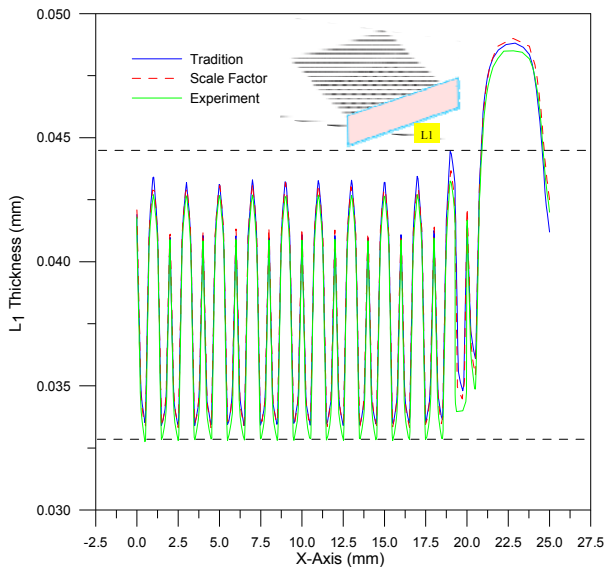


Fig. 8. The thickness distribution of L1 section (X-axis).

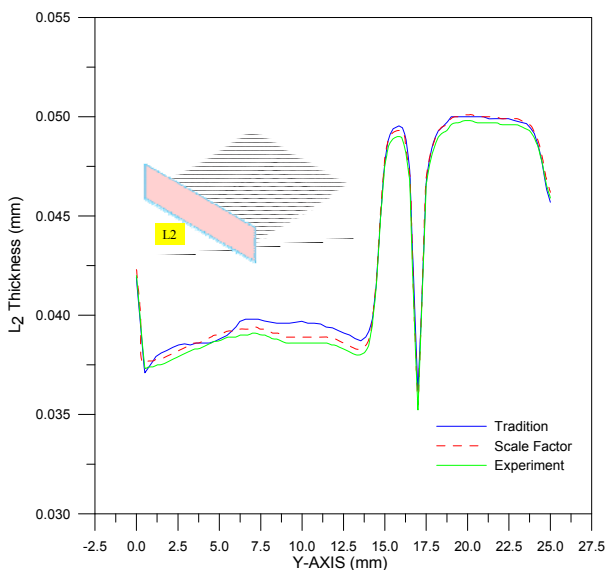


Fig. 9. The thickness distribution of L2 section (Y-axis).

Fig. 10 shows the shape comparison of L1 section. Although the differences of the thickness distribution on both material models and the experimental result were not obvious, there was significant difference on the bottom of the channel. The channel depth of the traditional material model was 0.45mm, and it was about 0.57mm of the scale-factor modified material model that was closer to the experiment with unload springback, 0.55mm. Aiming at L2 section, the shape comparison is shown as Fig. 11. The three (traditional material model, modified material model, and experimental result) presented obvious differences on the bottom of the channel. There was 0.13mm difference between the two models; and, the channel depth of the scale-factor modified material model was closer to the experimental result. In this case, it was proved that the micro-stamping process of sheet metal bipolar plates could be effectively simulated with finite element analysis and scale-factor modified material model.

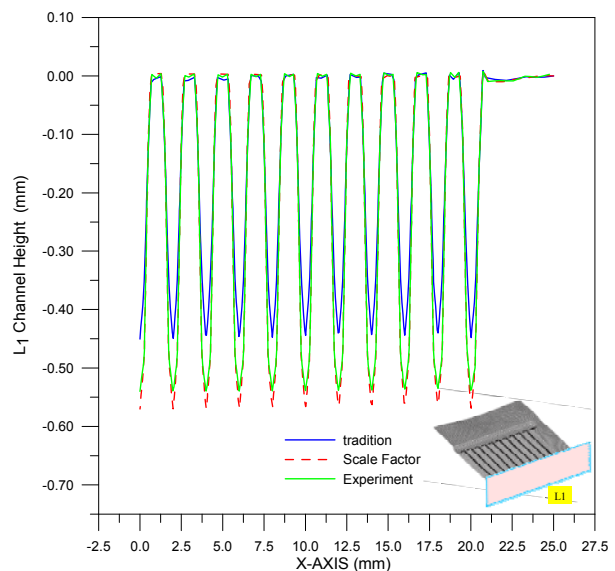


Fig. 10. The shape comparison of L1 section.

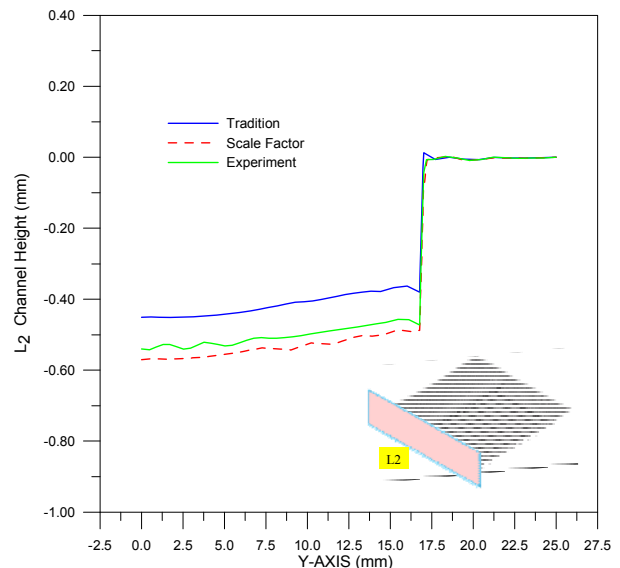


Fig. 11. The shape comparison of L2 section.

5. Conclusions

With elastic-plastic finite element analysis and thickness scale-factor modification, the micro-stamping process for sheet metal bipolar plates was studied. In terms of nonlinear management, an increment was applied for calculation; and, with r-minimum to limit the distance between increments, the calculation became linear relation. With the finite element simulation, the following conclusions were obtained.

1. With finite element analysis, the complete deformation process of the sheet metal bipolar plate micro-stamping process could be accurately analyzed, meaning that the entire deformation history could be drawn successfully.
2. In micro-forming process, the analysis result of the modified material model was closer to the experimental result.
3. At the round corners on the transverse channel of the bipolar plate, crackers were likely to appear that the radius of the round corner should be adjusted. The least thickness of the bipolar plate appeared on the top of the channel that it could be designed as an arc to avoid crackers.
4. Since the tools shape was drawn by CAD software, the developed finite element analysis model could be

applied to any other tools shapes for normal micro-pressing process.

Acknowledgment

This paper was supported by the National Science Council, Taiwan, Republic of China, through Grant NSC 98-2221-E-167-001. We are grateful to the National Center for High-performance Computing for computer time and facilities.

REFERENCES

- [1] Bar-On I., Kirchain R., Roth R., Technical cost analysis for PEM fuel cells, *J. Power Sources*, 109 (2002), 71-75
- [2] Tawfika H., Hung Y., Mahajan D., Metal bipolar plates for PEM fuel cell - A review, *J. Power Sources*, 163 (2007), 755-767
- [3] Hermann A., Chaudhuri T., Spagnol P., Bipolar plates for PEM fuel cells: A review, *Int. J. of Hydrogen Energy*, 30 (2005), 1297-1302
- [4] Li X., Sabir I., Review of bipolar plates in PEM fuel cells: Flow-field designs, *Int. J. of Hydrogen Energy*, 30 (2005), 359-371
- [5] Koç M., Mahabunphachai S., Feasibility investigations on a novel micro-manufacturing process for fabrication of fuel cell bipolar plates: Internal pressure-assisted embossing of microchannels with in-die mechanical bonding, *J. Power Sources*, 172 (2007), No. 2, 725-733
- [6] Wang S., Peng J., Lui W., Zhang J., Performance of the gold-plated titanium bipolar plates for the light weight PEM fuel cells, *J. Power Sources*, 162 (2006), 486-491
- [7] Mahabunphachai S., Koç M., Fabrication of micro-channel arrays on thin metallic sheet using internal fluid pressure: Investigations on size effects and development of design guidelines, *J. Power Sources*, 175 (2008), No. 1, 363-371
- [8] Lipman T. E., Edwards J. L., Kammen, D. M., Fuel cell system economics: comparing the costs of generating power with stationary and motor vehicle PEM fuel cell systems, *Energy Policy*, 32 (2004), 101-125
- [9] Matsuura T., Kato M., Hori M., Study on metallic bipolar plate for proton exchange membrane fuel cell, *J. Power Sources*, 161 (2006), 74-78
- [10] Peng L., Hu P., Lai X., Mei D., Ni J., Investigation of micro/meso sheet soft punch stamping process - simulation and experiments, *Materials and Design*, 30 (2009), 783-790
- [11] McMeeking R. M., Rice J. R., Finite element formulations for problems of large elastic-plastic deformation, *Int. J. Solids Structures*, 11 (1975), 601-606
- [12] Hinton E., Owen, D. R., *Finite Element Software for Plates and Shell*, Pineridge, Swansea, UK (1984)
- [13] Hughes T. J. R., *The Finite Element Method*, Prentice-Hall, Englewood Cliffs, NJ (1987)
- [14] Hughes T. J. R., Generalization of Selective Integration Procedures to Anisotropic and Nonlinear Media, *Int. J. Numerical Methods in Engineering*, 15 (1980), 1413-1418
- [15] Peng L., Liu F., Ni J., Lai X., Size effects in thin sheet metal forming and its elastic-plastic constitutive model, *Material and design*, 28 (2007), 1731-1736
- [16] Oden J. T., Pries E. B., Nonlocal and nonlinear friction law and variational principles for contact problems in elasticity, *J. Applied Mechanics*, 50 (1983), 67-76
- [17] Saran M. J., Wagoner R. H., A consistent implicit formulation for nonlinear finite element modeling with contact and friction: part I—theory, *Trans. ASME, Journal of Applied Mechanics*, 58 (1991), 499-506
- [18] Yamada Y., Yoshimura N., Sakurai T., Plastic Stress Strain Matrix and its Application for the Solution of Elastic-plastic Problems by the Finite Element Method, *Int. J. Mech. Sci.*, 10 (1968), 343-354

Authors: Tsung-Chia CHEN and Jiun-Ming YE are with the Department of Mechanical Engineering, National Chin-Yi University of Technology, Taichung, Taiwan.
(E-mail: ctchen@mail.ncut.edu.tw; bliming_model@gmail.com).